Preprints of the 21st IFAC World Congress (Virtual)
Berlin, Germany, July 12-17, 2020

Motion-blur Compensation System Using a Rotated Acrylic Cube with Visual Feedback

T. Hayakawa * **H. Nakane** ** **M. Ishikawa** ***

* *The University of Tokyo, Bunkyo-ku, Tokyo 113-8656, Japan (e-mail: tomohiko_hayakawa@ipc.i.u-tokyo.ac.jp).*
** *The University of Tokyo, Bunkyo-ku, Tokyo 113-8656, Japan (e-mail: haruka_nakane@ipc.i.u-tokyo.ac.jp)*
*** *The University of Tokyo, Bunkyo-ku, Tokyo 113-8656, Japan (e-mail: masatoshi_ishikawa@ipc.i.u-tokyo.ac.jp)*

Abstract: In an imaging system, motion blur occurs in an image when the target moves relative to the system, whereas there are restrictions and problems related to the long exposure time required by the method and the post-processing required after image processing. Therefore, in this research, we use the phenomenon by which the optical axis passing through an acrylic cube installed between the camera and the imaging target moves in parallel with the target's motion based on the difference in refractive index and Snell's law by rotating the cube. Thus, we propose a method to compensate for motion blur which is possible to capture the target's image as if it is still at each right angle of rotation. Furthermore, we proposed a visual feedback method that can compensate for motion blur accurately for an unknown target speed by using a Laplacian filter and the template matching, as well as a constant speed. It was confirmed that the motion blur was significantly mitigated in the experiment at a speed between 0 to 556 mm/s. Our result can be applied for the inspection systems which can capture target's image precisely with high efficiency.

Keywords: Image motion compensation, motion blur, acrylic cube, image processing, target tracking, velocity control, angular velocity.

1. INTRODUCTION

In fields that require extensive inspection, such as transportation infrastructure, production line quality control, and circuit board fabrication, it is important to check for faults and early failures with high accuracy and high efficiency to reduce costs and improve safety (see Richards (1998)). In particular, it is often necessary to acquire images with high spatial resolution, even when the relative speed between the target and the camera is high. This is problematic owing to the motion blur that occurs during imaging. There are several ways to suppress motion blur, including shortening the exposure time by using strong lighting, as shown in Masuzoe (2018), and using post-processing such as blind deconvolution, as shown in Yitzhaky et al. (1999) and Zhang et al. (2009). However, the former faces problems such as deterioration or deformation of the target due to strong lighting, whereas the latter has compatibility difficulties with real-time applications due to the introduction of artifacts and increased computational complexity. Consequently, in Inoue et al. (2017) and Hayakawa et al. (2015), clear images were captured even in a high-speed motion environment with an extended exposure time by controlling the optical axis using the high-speed reciprocal motion of a single-axis galvanometer mirror. However, these methods had reduced tracking performance and exposure time owing to the back-and-forth motion of the mirror, yielding lower imaging accuracy and quality.

This study proposes a efficient motion blur compensation system that can utilize a long exposure time and enable real-time tracking to utilize Snell's law and a rotated acrylic cube without the back-and-forth motion.

2. MOTION-BLUR COMPENSATION SYSTEM

2.1 Motion-blur compensation using a rotated acrylic cube

The purpose of this study is to construct a motion blur compensation system that controls the optical axis by using a rotating acrylic cube. Related to our method, Fox (1988) proposed a deconvolution method using a cube based on reflection; however, our method is based on refraction.

Fig. 1 depicts a schematic of our system. Motion correction is performed by rotating a transparent cube with a refractive index that differs from atmospheric conditions, thereby making the optical axis travel horizontally. In this work, the surface of the target to be imaged is assumed to be parallel to the sensor imaging surface. A geometrical optics approach is taken to calculate the traveling speed of the optical axis from the rotational speed of the cube. As shown in Fig. 2, if the refractive index of the cube in relation to the atmosphere is n, the length of one side of

Copyright lies with the authors

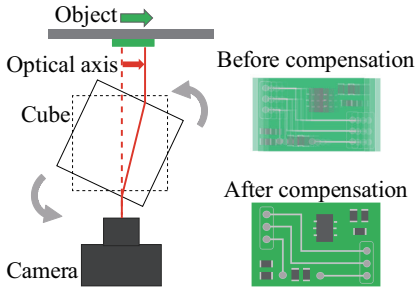

Fig. 1. Diagram of the proposed system

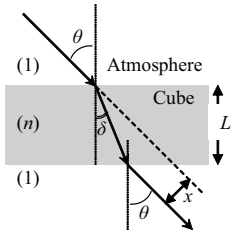

Fig. 2. Relationship between the angle of incidence and the travel distance of the optical axis during cube rotation

the cube is L, the angle of incidence to the cube is θ, the refraction angle is δ, and the displacement of the optical axis is x. Eq. 1 and Eq. 2 are found using Snell's law.

$$\sin\theta = n\sin\delta \tag{1}$$

$$x = L\frac{\sin(\theta-\delta)}{\cos\delta} \tag{2}$$

Eq. 3 is derived by substituting Eq. 1 into Eq. 2 and simplifying it by using trigonometric addition formulas.

$$x = L\sin\theta\left(1-\frac{\cos\theta}{\sqrt{n^2-\sin^2\theta}}\right) = f(\theta) \tag{3}$$

Eq. 4 is obtained if the angular velocity of the rotating cube is given by $\frac{d\theta}{dt} = \omega$ rad/s, and the velocity of the optical axis is v cm/s.

$$v = \frac{df}{d\theta}\omega \tag{4}$$

Therefore, when the speed of the target being imaged is known, the speed of the optical axis can be controlled so as to cancel the speed of the target by adjusting the rotation speed of the cube. Motion blur can then be compensated for by making the relative speed between the image of the target and the camera close to zero. In addition, because this system can capture images of all parts of the cube other than its corners, the upper limit of the exposure time is the time for the cube to make a 1/4 rotation, making it possible to image with a long exposure time.

2.2 Visual feedback algorithm for setting the rotation speed

We propose the method to adjust rotation speed when the velocity is unknown. The rotation speed was adjusted with the following 2-step algorithm.

(i) As shown in Figs. 3 and 4, the rotation speed is varied at a constant step interval and the images obtained at each rotation speed is multiplied with a Laplacian filter to calculate the variance. A smaller variance value implies more blurring of the image. Therefore, we search for the rotational speed corresponding to the image with the largest variance value. In Fig. 4, the initial rotation speed ω_i is set to 600 deg/s.

(ii) After setting the initial rotation speed ω_i, we acquire two images in succession, where the first is used as a template image, and the second is used for template matching. If the second image moves in the direction that the cube rotates, the rotation speed ω increases owing to the calculated speed by the image processing, and if it moves in the opposite direction, the rotation speed ω decreases owing to it. This process is realized in Eq. 5. ω is given by a proportional coefficient k and the pixel difference between 2 images based on the template matching. These calculation and processing is done in real-time.

$$\omega = \omega_i + kp_d \tag{5}$$

If the range of possible speeds of the target is small, the rotation speed may be adjusted using template matching in the second step from the beginning, but if the range of possible speeds of the target is large, the motion blur will be large. Since the template matching cannot be used, the approximate rotation speed is determined in step (i) and fine adjustment is performed in step (ii). Note, if the target speed changes quickly at each capture, the rotation speed will not match with the target speed.

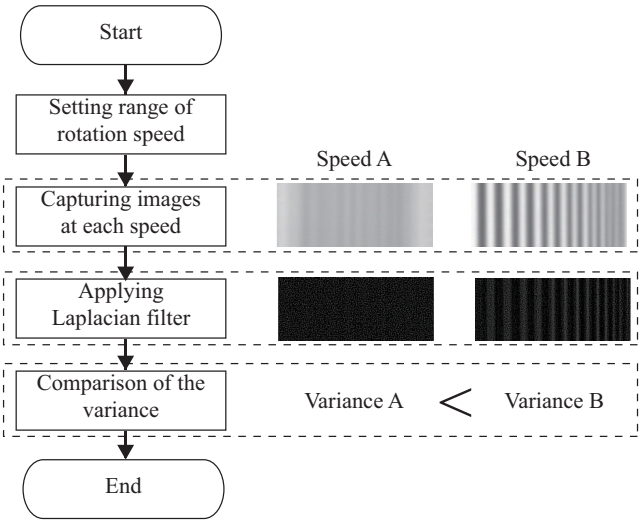

Fig. 3. Flowchart of imaging and image processing algorithms to determine the initial rotation speed

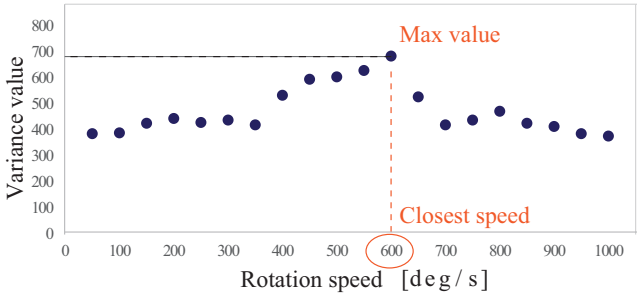

Fig. 4. Relationship between the variance value and rotation speed

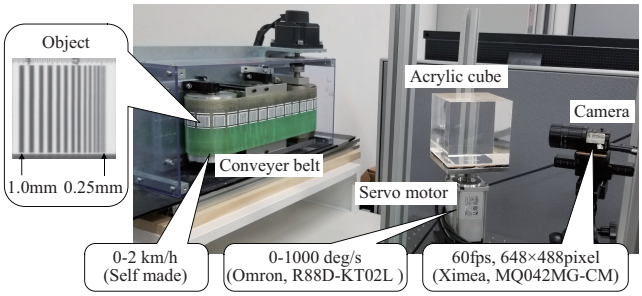

Fig. 5. Experimental setup and each hardware parameter

3. EXPERIMENT USING A CONVEYER BELT

The following experiment verified the method of the compensation of motion blur by using a rotating cube. In addition, it demonstrates the possibility of real-time optimization by automatically matching the rotation speed of the cube to various speeds of the target and comparing the image quality.

3.1 Experimental setup

The target is a black and white striped pattern (see Fig. 5) with stripe widths ranging from 1.0 mm to 0.25 mm, and it moves on a belt conveyor. An acrylic cube with a refractive index of 1.49 rotates on a servomotor (Omron, R88D-KT02L), and monochrome images are taken through the acrylic cube using a CMOS camera (Ximea MQ042MG-CM). The speed of the target is fixed at 97.2, 181, 278, 333, 417, 500, and 556 mm/s, the camera exposure time is 16.6 ms (60 fps frame rate), each side of the cube has a length of 10 cm, and the distance between the camera and the target is 50 cm.

3.2 Experimental results and discussion

As shown in Fig. 6 (b) and (c), a qualitative comparison of the image reveals that there is less motion blur after compensation than before compensation for a conveyer belt at the speed of 181 mm/s. Moreover, the image of the target while still and that after blur compensation are very similar (see Fig. 6 (a) and (c)). This can also be seen from Fig. 6 (d), which plots the intensity of the camera brightness along a straight line perpendicular to the stripe pattern in each image. Importantly, unlike Inoue et al. (2017) and Hayakawa et al. (2015), our result is achieved without back-and-forth motion, so the efficiency of the compensation raised.

To quantify the accuracy of blur compensation, the peak-to-peak value of the intensity of the camera brightness I_{pp} is defined as the difference between the minimum brightness of the third black line and the maximum brightness of the fourth white line from the left. As can be seen in Fig. 6 (d), the larger the value, the greater the contrast and the lower the blur. On the other hand, when the value is smaller, the blur is greater. Fig. 7 plots the results before and after blur compensation, with the horizontal axis representing traveling speed and the vertical axis representing I_{pp}. The I_{pp} value was obtained from the image, and it was corrected with the rotation of the acrylic cube. As expected, the blur increases as

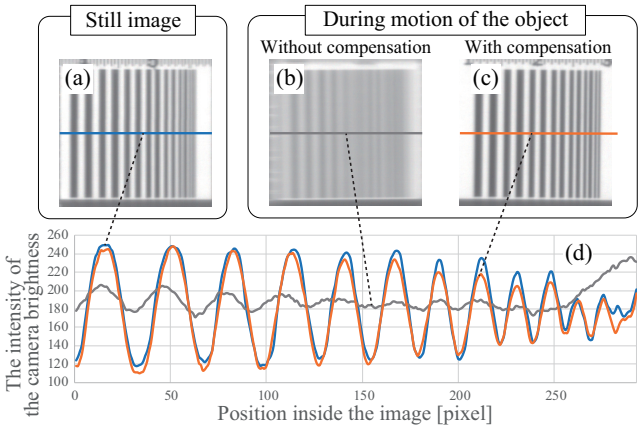

Fig. 6. Acquired images: (a) Stationary, (b) Before blur compensation, (c) After blur compensation, (d) Change in brightness across the striped pattern when the target speed is 181 mm/s

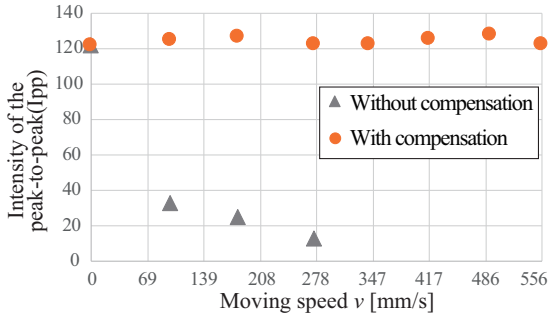

Fig. 7. Relationship between I_{pp} and traveling speed

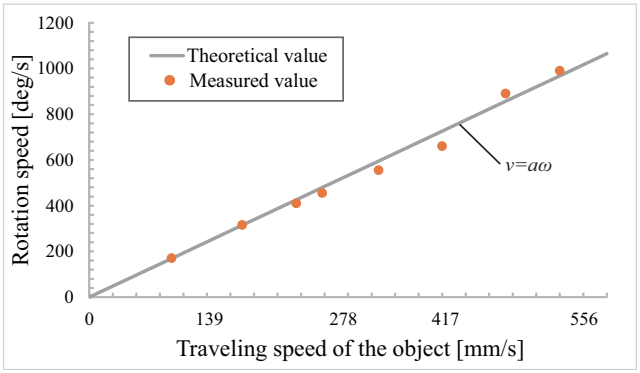

Fig. 8. Relationship between the theoretical and measured values of traveling speed and rotation speed

the speed increases without compensation whereas the compensated images retain a high I_{pp} value. Subsequently, the blur compensation was observed to be working well, regardless of the speed of the target (See Fig. 7).

Furthermore, as shown in Fig. 7 and 8, the rotation speed can be estimated at any speed after compensation, without an image of inferior quality to the still image. Specifically, Fig. 8 depicts the difference between the theoretical and measured single values at each speeds.

The theoretical values are plots of the equation of $v = a\omega$, where a is the slope of the tangent at the point $\theta = 0$ in Eq. 3. At that time, we set the parameters as follows:

$L = 100mm$, $n = 1.49$ as an image was acquired when the incident angle was approximately 0 degree in the experiment.

In addition, the measured values are determined using a method that adopts the maximum variance in algorithm (i) of Sec. 2.2, and then the rotation speed at the point of convergence is plotted for each target speed by applying the template matching method of algorithm (ii). The resultant RMSE value was 32.41 deg/s. From these plots and RMSE values, it is observed that the measured values do not greatly deviate from the theoretical values.

This result indicates that motion-blur compensation can be achieved even when the speed of the target is unknown by using visual feedback. The convergence time is not accounted for in this experiment; however, by automating the procedure, it is conjectured that compensation is possible, even when the speed of the target changes suddenly. Therefore, the proposed method was validated.

In the future, we will apply our method not only for black-and-white patterns, but also for more general textures. Subsequently, we plan to substitute our method with conventional motion-blur compensation method by using a galvanometer mirror of Hayakawa et al. (2018) for the efficient inspection system of traffic infrastructures. Additionally, we will update the target speed until 100 km/h at maximum to correspond with the inspection of the express ways to use a high-speed servo motor.

4. CONCLUSION

This study proposes a method to compensate for motion blur by controlling an optical axis via a rotating cube; we also validated it through an experiment. Furthermore, although the convergence time is required to calculate a precise speed, the experiment verified that motion blur compensation can be performed accurately even when the speed of the target is unknown, and it exhibited its potential for real-time motion blur compensation. This result can be applied for the inspection systems which capture target's image precisely with high efficiency, however, this system needs to correspond with higher target's speed as future work using a faster servo motor.

REFERENCES

Fox, J.S. (1988). Range from translational motion blurring. In *Proceedings CVPR '88: The Computer Society Conference on Computer Vision and Pattern Recognition*, 360–365. doi:10.1109/CVPR.1988.196260.

Hayakawa, T., Moko, Y., Morishita, K., and Ishikawa, M. (2018). Pixel-wise deblurring imaging system based on active vision for structural health monitoring at a speed of 100 km/h. In *Proceedings of the SPIE, Volume 10696*, 24:1–24:7.

Hayakawa, T., Watanabe, T., and Ishikawa, M. (2015). Real-time high-speed motion blur compensation system based on back-and-forth motion control of galvanometer mirror. *Opt. Express*, 23(25), 31648–31661. doi: 10.1364/OE.23.031648.

Inoue, M., Jiang, M., Matsumoto, Y., Takaki, T., and Ishii, I. (2017). Motion-blur-free video shooting system based on frame-by-frame intermittent tracking. *ROBOMECH Journal*, 4(1), 28. doi:10.1186/s40648-017-0096-0.

Masuzoe, K. (2018). Evaluation of soundness assessment of tunnel walls by mimm : We measure tunnels while running at 50km/h by using mimm and can find abnormality points. *Journal of the Japanese Society for Non-destructive Inspection*, 67(3), 118–121.

Richards, J. (1998). Inspection, maintenance and repair of tunnels: international lessons and practice. *Tunnelling and Underground Space Technology*, 13, 369–375.

Yitzhaky, Y., Milberg, R., Yohaev, S., and Kopeika, N.S. (1999). Comparison of direct blind deconvolution methods for motion-blurred images. *Appl. Opt.*, 38(20), 4325–4332. doi:10.1364/AO.38.004325.

Zhang, J., Zhang, Q., and He, G. (2009). Blind deconvolution of a noisy degraded image. *Appl. Opt.*, 48(12), 2350–2355. doi:10.1364/AO.48.002350.